Science of the Total Environment 790 (2021) 148090

Contents lists available at ScienceDirect

Science of the Total Environment

journal homepage: www.elsevier.com/locate/scitotenv

Benchmarking of drought and climate indices for agricultural drought monitoring in Argentina

Ronnie J. Araneda-Cabrera [a,*], María Bermúdez [b], Jerónimo Puertas [a]

[a] Water and Environmental Engineering Group (GEAMA), University of A Coruña, Civil Engineering School, Campus de Elviña, 15008 A Coruña, Spain
[b] Environmental Fluid Dynamics Group, Andalusian Institute for Earth System Research, University of Granada, Av. Del Mediterráneo s/n, 18006 Granada, Spain

HIGHLIGHTS

- El Niño 3.4 and 4 climate indices (CIs) are best correlated with drought indices (DIs).
- The spatial patterns of CI-DI correlations can be used to define homogenous drought regions.
- DIs were better predictors of soybean yield variability than CIs.
- SPEI-6 and SVHI-6 indices were the best DIs in explaining the variability of soybean yields.
- A foundation is laid for finding suitable indicators for the forecasting of drought.

GRAPHICAL ABSTRACT

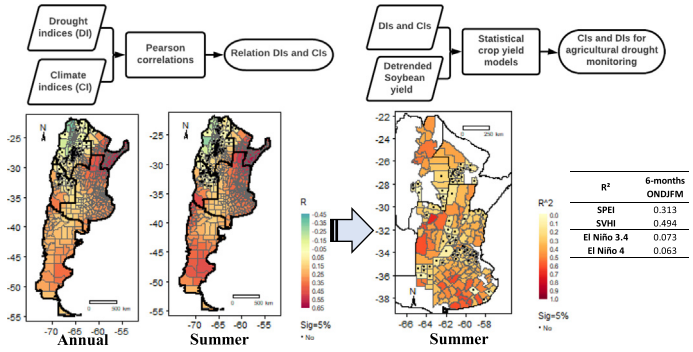

ARTICLE INFO

Article history:
Received 12 March 2021
Received in revised form 9 May 2021
Accepted 24 May 2021
Available online 28 May 2021

Editor: Fernando A.L. Pacheco

Keywords:
Drought indices
Agricultural drought
Teleconnections
Statistical models
Soybean yield.

ABSTRACT

Site-specific studies are required to identify suitable drought indices (DIs) for assessing and predicting drought-related impacts. This study presents a benchmark of eight DIs and 19 large-scale climate indices (CIs) to monitor agricultural drought in Argentina. First, the link between the CIs and DIs was investigated at the departmental-administrative level and at different temporal scales. Then, the effectiveness of the DIs in explaining the variability of crop yields, understood as impacts of agricultural droughts, was evaluated using statistical regression models. Soybeans were used as the reference crop. Additionally, the performances of DIs and CIs in explaining the variability of crop yields were compared. The CIs located in the Pacific Ocean (El Niño 3.4 and El Niño 4) were found to have the best correlations with the DIs (R values up to 0.49). These relationships were stronger with longer temporal aggregations and during the wet and hot seasons (summer), showing a significant role in the triggering of droughts in Argentina. The DIs that best corelated with CIs were those that included temperature in their calculations (STCI, SVHI, and SPEI). The impacts of droughts on soybean production were better explained using DIs than with CIs (up to 89% vs 8% of variability explained) as predictors of the statistical models. SVHI-6 and SPEI-6, depending on the area of interest, were, during the phenological period of crop growth (summer), the most effective DIs in explaining annual variations in soybean yields. The results may be of interest in water resource management, drought risk management, and the Argentinean soybean production sector. Furthermore, they provide a foundation for future studies aimed at forecasting agricultural droughts and their impacts.

1. Introduction

Drought is a natural stochastic hazard that causes substantial socio-economic and environmental losses worldwide (Golnaraghi et al., 2014). It is a complex phenomenon, usually initiated when precipitation

* Corresponding author at: Water and Environmental Engineering Group (GEAMA), University of A Coruña, Civil Engineering School, Campus de Elviña, 15008 A Coruña, Spain.
E-mail address: ronnie.aranedac@udc.es (R.J. Araneda-Cabrera).

https://doi.org/10.1016/j.scitotenv.2021.148090

presents with volumes below normal in a particular place (meteorological drought). Such anomalies go on to affect agriculture and hydrology (agricultural and hydrological drought, respectively), an issue reviewed in Mishra and Singh (2010). To date, several drought indices (DIs) have been developed with the intention of characterising and monitoring the phenomenon (World Meteorological Organization and Global Water Partnership, 2016; Zargar et al., 2011). These include the Standardised Precipitation Index (SPI; McKee et al., 1993) and the Standardised Precipitation Evapotranspiration Index (SPEI; Vicente-Serrano et al., 2010) for meteorological droughts, the Vegetation Condition Index (VCI) and the Vegetation Health Index (VHI; Kogan, 1995) for agricultural droughts, the Standardised Streamflow Index (SSI; Hao and AghaKouchak, 2013), plus the Palmer Hydrological Severity Index (PHSI; Palmer, 1965; Zargar et al., 2011) for hydrological droughts. Each DI has advantages and disadvantages, which have been discussed in previous studies (Keyantash and Dracup, 2002; Mishra and Singh, 2010).

Since the introduction of the concept of a drought timescale by McKee et al. (1993), DIs have been used to quantify drought events in each component of the terrestrial water cycle (e.g. precipitation, soil moisture, and groundwater). In turn, these DIs can be associated with certain water uses (e.g. agriculture and electric generation) (Guttman, 1998). Agricultural activity, on which food security and much of the global economy depends, has increased significantly in recent years due to the growing demand for food by an increasing population (Tester and Langridge, 2010). However, growth in farming has not been linear in time, as annual variations have been characterised by significant decreases in production. Although crop yields can be affected by a variety of factors, including wars, social crises, and plagues, drought is a key factor in yield variability, especially for rainfed crops (Leng and Hall, 2019; Lobell et al., 2011a, 2011b; Zampieri et al., 2017). Several studies have successfully correlated DIs with variability in crop yields worldwide (Araneda-Cabrera et al., 2021; García-León et al., 2019; Peña-Gallardo et al., 2019a; Quiring and Papakryiakou, 2003; Vicente-serrano et al., 2012). Generally, these relationships are assessed using statistical models (Shi et al., 2013). DIs can thus be used as predictors of crop yields in such models and may explain the impact of agricultural drought.

Drought variability can be linked to large-scale climate oscillations (Hassan and Nayak, 2020; Singh, 2012), which are quantified by climatic indices (CIs) that rely on sea surface temperature (SST) and sea pressure level (SPL). Some well-known CIs based on SST are the ENSO indices (in the Pacific Ocean: The El Niño 3.4, for instance), the Caribbean Index (CAR; in the Caribbean Sea), and the south-eastern tropical Indian Ocean (SETIO; in the Atlantic Ocean). On the other hand, CIs based on SPL include Darwin and Tahiti (in the Pacific Ocean) and North Atlantic Oscillation (NAO; in the Atlantic Ocean) in the Atlantic Ocean. Several studies have linked climate indices to DIs (Huang et al., 2016; Manatsa et al., 2008; Oñate-Valdivieso et al., 2020; Santos et al., 2019). Other studies have used climate indices to forecast droughts (Dutra et al., 2013; Tan and Perkowski, 2015).

Because variability in crop yields can be related to DIs, which in turn can be linked to CIs, some studies have directly connected crop yield variability with CIs (Anderson et al., 2017; Iizumi et al., 2014; Leng and Hall, 2019; Wang et al., 2020). Correlations between crop yields and CIs are usually lower than those with DIs, although no research which specifically addresses and supports this assertion currently exists. For instance, in the United States, Anderson et al. (2017) found correlations between soybean yield and the Oceanic Niño Index (ONI) of up to $r = 0.30$, while Peña-Gallardo et al. (2019b) highlighted correlations between the same crop yield and the SPEI of as much as $r = 0.70$.

There is no single DI that can explain variability in crop yields (i.e., drought-related impacts on agricultural production). Similarly, there is no single CI (teleconnection) that can represent all climate variability and can thus be used to predict drought conditions over large regions (Stenseth et al., 2003). This is due to the very large differences in environmental physical factors (climate, soil composition, topography, etc.) that make both climate and crop development respond differently in each location. Hence, the present study compares the performance of eight DIs and 19 CIs to determine which are the most appropriate for use in agricultural drought monitoring throughout Argentina.

Argentina has the highest per capita crop production in the world (FAO, 2019) and is also the third largest soybean producer (Food and Agriculture Organization, FAO; http://faostat.fao.org). The country has substantial annual and inter-annual climate variability (Barros and Silvestri, 2002), and the likelihood of soybean yield reduction due to droughts ranges from 70 to 81% (when experiencing moderate to exceptional droughts, respectively) (Leng and Hall, 2019). In Argentina, DIs have been related to crop variability (e.g. D'Ambrosio et al., 2013; Seiler et al., 2007) and to CIs (e.g. Díaz et al., 2018; Rivera et al., 2018; Vicario et al., 2015) for specific regions, such as certain provinces or river basins. Similarly, relationships have been established between some crop yields and CIs, but only for specific regions (e.g. Anderson et al., 2017; Iizumi et al., 2014; Podestá et al., 1999). However, to the best of the authors' knowledge, there are no studies that benchmark different DIs and large-scale CIs for explaining agricultural drought and associated crop variability.

The goals of this study are: a) to determine which climate index (or indices) is best associated with droughts and with which drought index; b) to establish a drought index (or a set of indices) that can explain the annual variability in crop yield using soybeans as a benchmark crop; and c) to compare drought and climate indices as predictors of crop yield variability through three statistical models. The study was conducted throughout the country at the level of administrative departments. The ultimate aim is to support decision makers, farmers, and agricultural drought managers in Argentina. However, the methodology can be applied to other countries or regions and at any spatial scale.

2. Materials and methods

2.1. Study area

Continental Argentina was defined as the case study (Fig. 1a). It covers 2,791,810 km^2 and is divided into five main administrative regions according to the National Institute of Statistics and Censuses Argentine Republic (Spanish acronym INDEC: www.indec.gob.ar), 24 provinces (including the Autonomous City of Buenos Aires as a province), and 525 departments (m number of departments) (Fig. 1b). Due to its extensive area, the country sees wide climatic diversity, from arid (south and centre-north) to fully humid (northeast) (Beck et al., 2018; Kottek et al., 2006). However, 55% of the country has drylands (Cherlet et al., 2018). Argentina is one of the major worldwide producers of cereals (FAO, 2017), which are cultivated largely in the Argentine Pampas. The departmental average annual precipitation varies between 70 and 1880 mm per year and, the average annual temperature ranges from 2 to 23 °C. Both precipitation and temperature increase from east to west and from south to north. The spring and summer seasons are the most humid, while autumn and winter are the coldest and driest. The value of Argentina's cereal production was $10.2 billion in 2013, representing 8.3% of its GDP (FAO, 2017). The country is vulnerable to several natural phenomena (earthquakes, floods, etc.); however, droughts represent the greatest risk for agricultural losses (Cherlet et al., 2018). Argentina's agricultural year is defined as July to June (https://www.argentina.gob.ar/agricultura-ganaderia-y-pesca), while the hydrological year varies across the country according to regional precipitation patterns. At the national level, the precipitation data used in this study (see Section 2.2) show that the driest month is June; therefore, in this study, the hydrological year was taken to coincide with the agricultural year.

2.2. Drought indices

Various indices based on meteorological, vegetation condition, and hydrological variables were calculated for each department on a

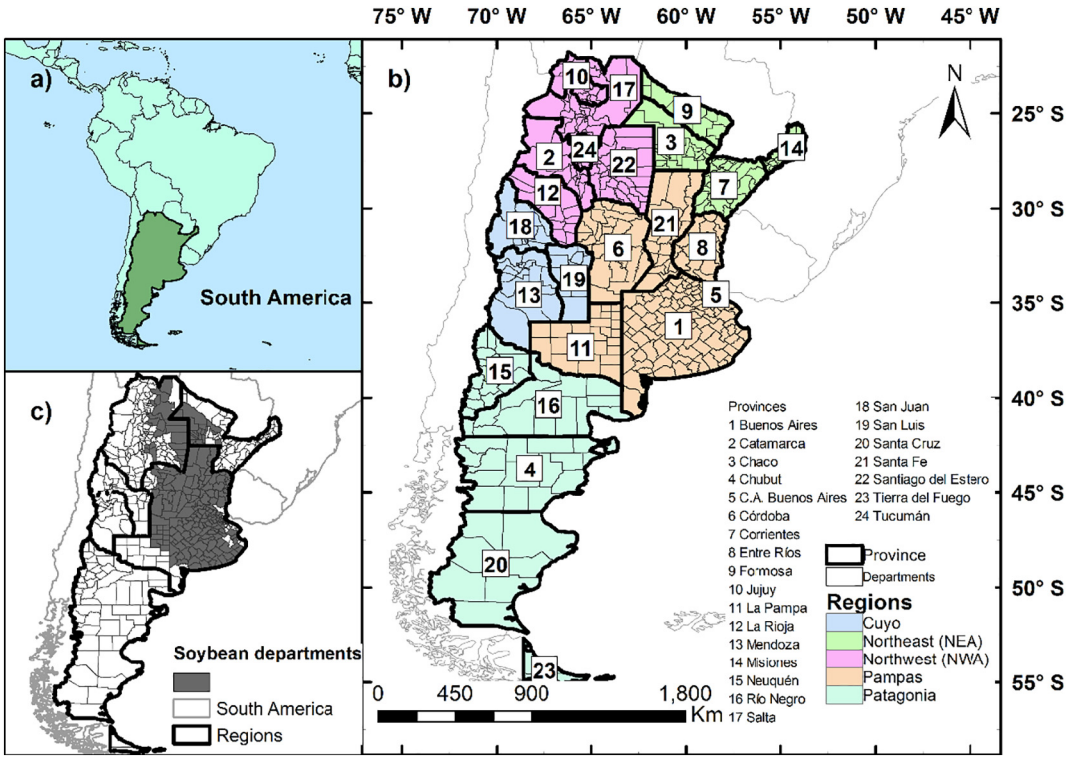

Fig. 1. Location of a) Argentina; b) regional, providence and department divisions; and c) departments with soybean production.

monthly scale: SPI, SPEI, SSI, SPDSI, SVCI, STCI, SVHI, and STWSI. Each index, together with its data source, is briefly described, as follows:

The Standardised Precipitation Index (SPI) is one of the best-known DIs and is recommended by the World Meteorological Organization (WMO). It was introduced by McKee et al. (1993). It is based on transforming precipitation into a normal function ($\bar{x} = 0$ and $\sigma = 1$) by means of a probability distribution function of two gamma parameters. It is very versatile because it can be calculated for any time scale *n*. The detailed procedure for its computation can be found in Kumar et al. (2009). Monthly precipitation data were downloaded from the TerraClimate database (Abatzoglou et al., 2018) at http://www.climatologylab.org/terraclimate.html at a spatial resolution of 1/24° (≈4 km at the equator) and were averaged for each department before calculating the SPI.

The Standardised Precipitation and Evapotranspiration Index (SPEI) was introduced by Vicente-Serrano et al. (2010). It is similar to the SPI, but is computed by standardising the water deficit (D = Precipitation − Evapotranspiration). Here, D is fitted to a three-parameter log-logistic function: precipitation and potential evapotranspiration series data were downloaded from the TerraClimate database and calculated for each department from the average prior to the computation of the SPEI.

The Standardised Soil Moisture Index (SSI) (Hao and AghaKouchak, 2014) is based on the standardisation of soil moisture following the mathematical steps of the SPI. Here, we used soil moisture obtained from the Climate Change Initiative (CCI) program of the European Space Agency (ESA) at https://www.esa-soilmoisture-cci.org, version v04.7, at a 0.25° spatial grid (Dorigo et al., 2017). These data were downscaled to the departmental level using a bilinear resampling of their centroids.

The Standardised Vegetation Condition Index (SVCI), Standardised Temperature Condition Index (STCI), and Standardised Vegetation Health Index (SVHI) (Agutu et al., 2017) were calculated following the standardisation procedure of the SPI to the VCI, TCI, and VHI time series, as defined by Kogan (1995). These data were downloaded from the Center for Satellite Applications and Research (STAR) and the Environmental Satellites for the U.S. Oceanic and Atmospheric Administration (NOAA) at https://www.star.nesdis.noaa.gov/smcd/emb/vci/VH/vh_ftp.php. Datasets consist of 7-day value composites at 8 km resolution that were averaged to monthly and departmental scales before being standardised.

The Standardised Palmer Drought Severity Index (SPDSI) (Ma et al., 2014) is the result of standardising the widely-used drought index PDSI (Palmer, 1965). The PDSI was downloaded from the TerraClimate database and averaged at the departmental scale. Then, the time series were processed according to the SPEI computing steps.

The Standardised Total Water Storage Index (STWSI) (Agutu et al., 2017) was computed using the SPEI procedure. Instead of D, the input is the total water storage anomaly (TWS) – surface water and groundwater – derived from the Gravity Recovery and Climate Experiment (GRACE) developed by the National Aeronautics and Space Administration (NASA) and the German Aerospace Centre (Landerer and Swenson, 2012). In this study, we used data (level water thickness in cm) provided by the Jet Propulsion Laboratory (JPL) as part of the GRACE Follow On mission JPL RL06_v02 (Landerer et al., 2020) at https://podaac.jpl.nasa.gov/dataset/TELLUS_GRAC-GRFO_MASCON_CRI_GRID_RL06_V2. Because the data are represented on a 0.5° grid, the time series were downscaled to the departmental scale using bilinear resampling towards their centroids prior to the standardisation procedure.

The datasets used in this study have been validated and used successfully in other drought-related studies (Araneda-Cabrera et al., 2020; Rojas et al., 2011; Thomas et al., 2014; Wang et al., 2019). The TerraClimate database offers data from January 1958; however, only the data since August 1981 were downloaded, so as to have the same time span as that offered by NOAA STAR. GRACE began its mission in April 2002; thus, we have data from that date. All variables were obtained up to December 2019. The DIs were calculated for seasonal and annual time scales (*n*) of 3, 6, and 12 months, since crop data that reflect agricultural droughts have sub-annual cycles (cf Section 2.4, below). Because of the aggregation of *n* months as part of the computation of the DIs, the time length of the DIs is *n* months less than their primary variables. Therefore, the final common timespan covered by the DIs was from August 1982 and April 2003 (STWSI) to December 2019. Some

data was missing for certain months due to technical problems (VCI, TCI, VHI, and TWS), and here a linear interpolation method was adopted to complete the data based on the neighbouring months. This method is effective and widely-used for handling missing data (Noor et al., 2015). As previously noted, the VCI, TCI, VHI, PDSI, and TWS variables were standardised according to the recommendations proposed for the calculation of the SPI and SPEI. In this way, all DI values could be interpreted in the same, with values below −0.5 indicating droughts with variable intensities (McKee et al., 1993).

2.3. Large-scale climatic indices

A wide variety of climate indices were considered in this study. These are based on the SST from the Atlantic (TNA, TSA, NAT, SAT, and TASI), Pacific (ENSO indices ERSSTv5: Niño 1 + 2, Niño 3, Niño 4, Niño3.4, and PDO), and Indian (SWIO, WTIO, SETIO, and DMI) Oceans, and SPL from various locations across the world (Darwin, Tahiti, SOI, and NAO). Additionally, we used the CAR associated with the SST from the Caribbean Sea. Thus, we used a total of 19 monthly aggregated climate indices that can be freely obtained in near real-time, the details of which are shown in Table 1. For this study, we downloaded the climate indices for the same time span as for the Dis, from August 1981 and April 2002 (STWSI) to December 2019. To establish consistency in the DIs, 3-, 6-, and 12-month running means were applied to the CIs.

2.4. Crop yield data

Annual crop yields at the departmental level were obtained from the Ministry of Agriculture, Livestock, and Fisheries of Argentina (Ministerio de Agricultura, Ganadería y Pesca de Argentina) at https://datos.agroindustria.gob.ar/dataset/estimaciones-agricolas. This database includes the sowed area, harvested area, and total production of 30 different crops from 1961 to 2019. Each year was measured from July to June (agricultural year). Soybeans were chosen as a representative rainfed crop because since 2000 it has been the cereal with the highest growth both in farmed areas and total production in the country. It is the most important crop in Argentina (Anderson et al., 2017; FAO, 2016; Leng and Hall, 2019; Magrin et al., 2005). The annual soybean yield (kg/Ha) was calculated by dividing production by the sowed area. All departments showing continuous series over time were considered, representing a total of 193 soybean-producing departments (Fig. 1c), where the annual yield data timespan was 16 years, from July 2004 to June 2019 (Fig. 2). In the case of soybeans, sowing is carried out from October to December, and harvesting from April to June. Notably, lower median and mean soybean yields were obtained in 2009 and 2018, years affected by significant drought episodes (EM-DAT, 2019).

Because crop yields are affected by factors other than climate, including agricultural innovations, technological improvements in sowing practices, and seed selection, crop yields generally have a positive trend (Peña-Gallardo et al., 2019b; Tian et al., 2018). This is also evident in Argentina; therefore, the yield series were detrended to remove the variability in productivity caused by non-climate factors using a linear regression model adjusted to the soybean yield series of each department. The average crop yield of each series was added to the residual model series to produce non-trend yield data in Kg/Ha (hereafter Y) following the procedure explained in detail in Lobell et al. (2011b) and used in other studies (e.g. Tian et al., 2018).

2.5. Relationship between drought indices and climatic indices

Pearson correlations (r) were calculated between CIs and DIs aggregated for 12 months at the departmental level throughout the country. Because the sign of the correlations is important (positive or negative indicate in-phase or anti-phase relation), r values were used instead of other metrics as the coefficient of determination (R^2). Then, a seasonal analysis was also performed with DIs and a selected number of CIs (in the previous step) with 6-month aggregations (for summer: March, for autumn: June, for winter: August, and for spring: December). Seasonal computing was performed for the entire country (m = 525) and for all soybean producing departments (m = 193). In the latter, we prioritised the summer analysis because this is the sowing and growing period for soybeans. The STWSI, with a shorter data length, may show better correlations with the CIs than the other DIs; thus, statistical significance will be a determining factor in the comparison of results.

2.6. Statistical crop yield models

To compare DIs as explanations for the variability of crop yields, we trained three statistical models (Lobell and Burke, 2010; Shi et al., 2013) over the 193 soybean producing departments: time-series, panel, and cross-section models. In all three cases, we assumed *Y* (in each department) was the response of a function of *k* independent variables *X*, which, in this context, are the DIs as possible predictors.

Table 1
Selected climatic indices and their free sources.

Variable/data set	Period available	Data availability
Darwin Sea Level Pressure (Darwin SLP)[a]	Jan 1882–now	http://cpc.ncep.noaa.gov/data/indices/darwin
Tahiti Sea Level Pressure (Tahiti SLP)[a]	Jan 1882–now	http://cpc.ncep.noaa.gov/data/indices/tahiti
Southern Oscillation Index (SOI)[b]	Jan 1866–now	https://psl.noaa.gov/gcos_wgsp/Timeseries/SOI/
ENSO indices (ERSSTv5): El Niño 1 + 2, El Niño 3, El Niño 4, and El Niño 3.4[a]	Jan 1950–now	https://cpc.ncep.noaa.gov/data/indices/ersst5.nino.mth.81-10.ascii
Pacific Decadal Oscillation (PDO)[b]	Jan 1948–Dec 2018	https://psl.noaa.gov/data/correlation/pdo.data
Caribbean Index (CAR)[b]	Jan 1950–now	https://psl.noaa.gov/data/correlation/CAR_ersst.data
South Western Indian Ocean (SWIO)	Nov 1981–now	https://stateoftheocean.osmc.noaa.gov/sur/ind/swio.php
Western Tropical Indian Ocean (WTIO)[b]	Jan 1870–now	https://psl.noaa.gov/gcos_wgsp/Timeseries/Data/dmiwest.had.long.data
Southeastern Tropical Indian Ocean (SETIO)[b]	Jan 1870–now	https://psl.noaa.gov/gcos_wgsp/Timeseries/Data/dmieast.had.long.data
Indian Ocean Dipole Mode Index (DMI)[b]	Jan 1870–now	https://psl.noaa.gov/gcos_wgsp/Timeseries/Data/dmi.had.long.data
Tropical Northern Atlantic Index (TNA)[b]	Jan 1948–now	https://psl.noaa.gov/data/correlation/tna.data
Tropical Southern Atlantic Index (TSA)[b]	Jan 1948–now	https://psl.noaa.gov/data/correlation/tsa.data
North Atlantic Tropical (NAT)[c]	Nov 1981–now	https://stateoftheocean.osmc.noaa.gov/sur/atl/nat.php
South Atlantic Tropical (SAT)[c]	Nov 1981–now	https://stateoftheocean.osmc.noaa.gov/sur/atl/sat.php
Tropical Atlantic (TASI)[c]	Nov 1981–now	https://stateoftheocean.osmc.noaa.gov/sur/atl/tasi.php
North Atlantic Oscillation (NAO)[b]	Jan 1950–now	https://psl.noaa.gov/gcos_wgsp/Timeseries/Data/nao.long.data

"a"; "b"; "c"; "d" specifies Source.
[a] Climate Prediction Center of NOAA.
[b] Physical Sciences Laboratory of NOAA.
[c] Ocean Observations Panels for Climate.

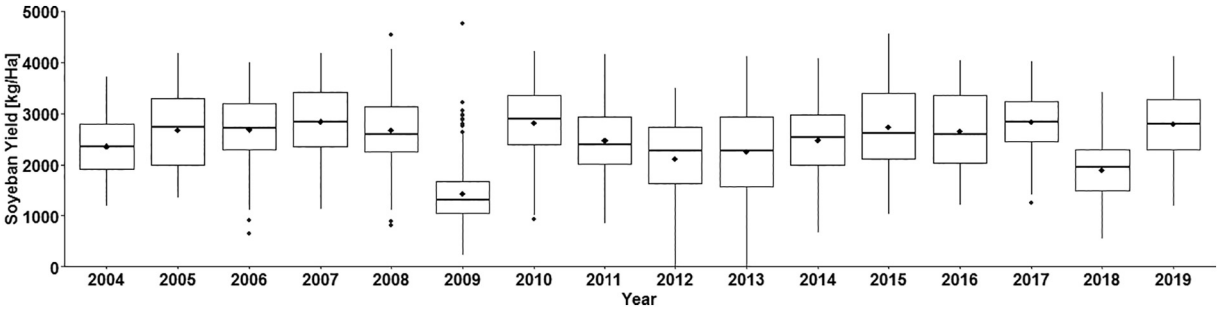

Fig. 2. Temporal series of detrended soybean yields for the 193 departments for the period 2004–2019. The solid black line shows the median, and the black dot shows the mean.

Given $Y \in [0,\infty)$, the time series model was implemented in each department as follows:

$$\ln(Y_t) = f(X_{t1}, X_{t2}, ..., X_{tk}) = \beta_0 + \sum_{j=1}^{k} \beta_j(X_{tj}) + \varepsilon_t, \quad (1)$$

where Y is the departmental vector of annual soybean yields, t is the year, X represents the vector of the candidate predictors, β_0 and β_j are the parameters (intercept and constant coefficients) to be fit, and ε is the error.

A panel regression model was executed combining the 193 departments:

$$\ln(Y_{i,t}) = \beta_{i,0} + \sum_{j=1}^{k} \beta_{i,j}(X_{i,tj}) + \varepsilon_{i,t}, \quad (2)$$

where i represents each soybean-producing department, and $\beta_{i,0}$ is an intercept.

Finally, the average departmental yields and DIs were computed to estimate the cross-sectional model.

$$\ln(Y_{i,avg}) = \beta_0 + \sum_{j=1}^{k} \beta_j(X_{i,avgj}) + \varepsilon_i \quad (3)$$

The predictor candidates were: the June DIs with a 12-month aggregation period, this for consistency with the annual crop yield data; the March DIs with a 6-month aggregation period, coinciding with the sowing and growing periods of soybeans; and the December and March DIs with a 3-month aggregation period, this to capture the sowing and growing periods of soybeans, respectively. The coefficients of determination of the models were used as the comparative statistics.

Moreover, to compare the performance of DIs and CIs as crop yield predictors, those CIs that showed the highest correlations with the DIs in the analysis described in Section 2.5 were evaluated as candidate predictors in the time-series model, following Eq. (1). A 3-, 6-, or 12-month running mean from June, March, or December was applied to the CIs for consistency with the DIs.

The overall procedure for identifying suitable DIs and CIs for monitoring agricultural drought in Argentina is summarized in Fig. 3.

3. Results

3.1. Identification of the large-scale climate drivers of drought

The spatiotemporal patterns of the correlations between CIs and DIs in Argentina were seen to vary significantly. The greater the temporal aggregation, the greater the correlations and the higher the percentage of departments with significant correlations (Table S1). Table 2 shows the correlations between the DIs and CIs with a 12-month aggregation. The STWSI showed the strongest correlation with all the CIs. However, some DIs (SPI, SPEI, STCI, SVHI, and SPDSI) showed a higher percentage of departments with significant correlations. The CIs that best correlated with all the DIs were Tahiti and SOI, with negative correlations, and El Niño 3.4 and El Niño 4, with positive correlations. These four CIs showed percentages of departments with statistically significant correlations of at least 74% ($\rho < 0.05$) and were selected for further analysis. The spatial patterns of the correlations between the DIs and selected CIs were similar (Figs. 4 and S1). DIs that included temperature in their calculus (STCI, SPEI, and SVHI) had the highest percentage of departments with significant correlations. The Pampas and NEA regions had the strongest negative correlations, followed by Cuyo and NWA with negative correlations, and finally Patagonia, where correlations were low and negative (Fig. 4). Table 3 shows the results of the correlations by region, which support the spatial patterns shown in Fig. 4 and S1.

A seasonal analysis was conducted correlating the seasonal series between the 6-month-aggregated DIs at the national level (Table S2 in the supplementary materials). The El Niño 3.4 and El Niño 4 had stronger correlations than did the other two indices. The SSI and STWSI showed stronger correlations for the cold seasons (winter and spring), while the rest of the DIs did so during the warmer seasons (summer

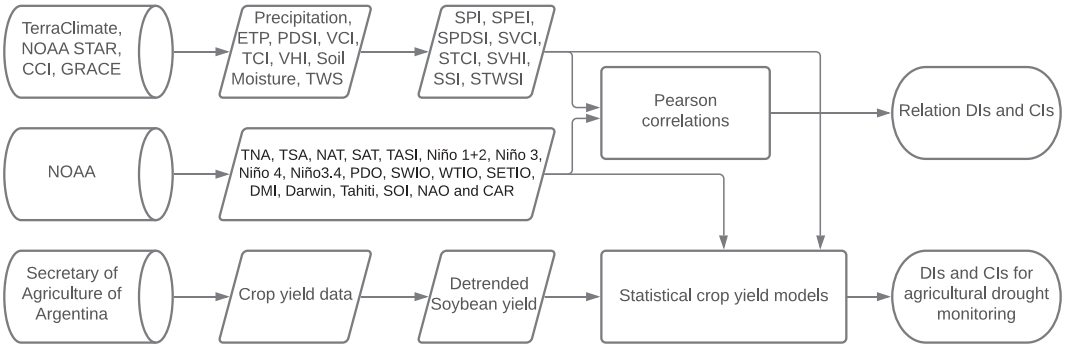

Fig. 3. Methodological flow-chart of the study.

and autumn). Persistent (very few exceptions) negative correlations during spring and summer and positive correlations during autumn and winter between El Niño 3.4 and the DIs were observed (Table S3). Similar patterns were observed for the other three selected CIs (Table S4 in the supplementary materials). Spatially, regions with weak correlations had the most departments with non-significant correlations, and this number increased in the winter and spring seasons. For example, Fig. 5 illustrates the spatial patterns of correlations between SPEI-6 and El Niño 3.4.

Considering only the soybean-producing departments and the summer season, when soybean sowing and growth occurs, the SPEI and STWSI had the strongest correlations with the four selected CIs (Table 4). For these specific departments and seasons, the r medians were persistently higher than the correlation found when all departments were considered. However, similar patterns were found in other seasons (Supplementary Table S5).

3.2. Comparison of the performance of DIs in explaining soybean yield variability

The results of the three statistical models with the soybean yield data and DIs are presented in Table 5. The determination coefficients (R^2) of the cross-section model were consistently higher than those of the other models. The SVHI, SVCI, STCI, SPEI, and SPI, which are based on meteorological and vegetation variables, better explained the variability of soybean yields in all three models and performed better using their 3- and 6-month aggregations for the summer season (in March) as a predictor. The other DIs (SSI, SPDSI, and STWSI) had a lower explanatory power and performed better with the 12-month aggregation in June.

The spatial distributions of the determination coefficients using the time-series model with predictors aggregated for six months are shown in Fig. 6. For all DIs, the models produced positive coefficients. This was not surprising, given that when DI values are lower (indicating more intense/severe drought events), reductions in crop (soybean) yields are expected. Specifically, the time-series model estimated positive coefficients in >96% of the departments (except SSI, which did so in 84%). The SVHI, which has the highest median determination coefficients, provided the best explanation of the variability of soybean yields in the central areas of the Pampas region. This zone obtained the highest R^2 values using any of the DIs as predictors. The SPEI was the best predictor of soybean yield in departments located in the southern and northern parts of the soybean belt.

3.3. Comparison of the performance of CIs in explaining soybean yield variability

Table 6 highlights the results of the time series models computed using the soybean yield data and four selected CIs (Tahiti, SOI, El Niño 3.4, and El Niño 4). Similar to the results with the DIs as predictors, the CI 3- and 6-months running-mean in summertime (March) explained the variability of soybean yields better than the CI 12-months running mean. The highest R^2 was found using El Niño 3.4 and El Niño 4. However, this maximum goodness of fit explained only 11.90% of the variability in soybean yield. In other words, the performance of CIs as possible predictors of soybean yield was very poor in Argentina for these specific timescales (6 and 12 months) and months (March and June).

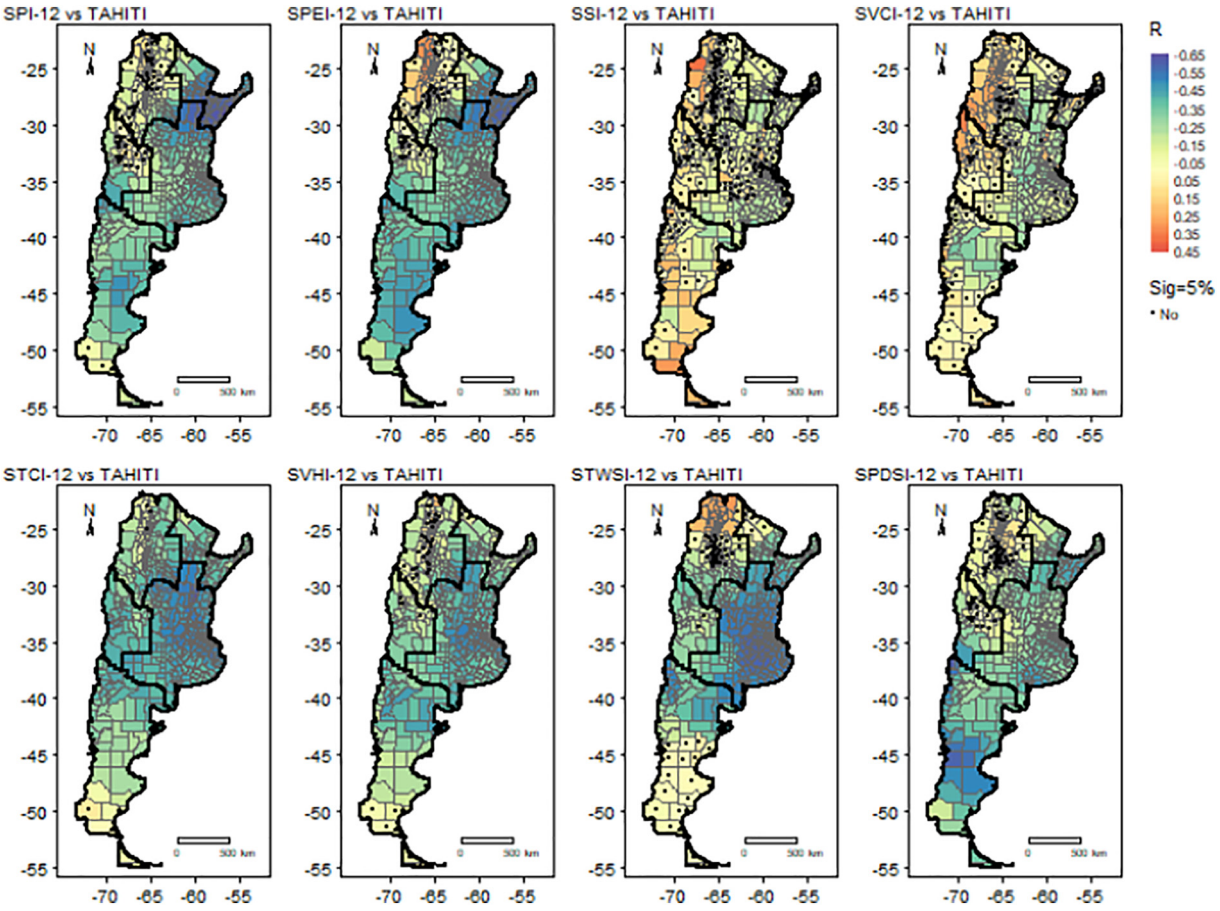

Fig. 4. Spatial pattern of correlations between the 8 DIs with a 12-month aggregation period and Tahiti SLP CI based on 1982–2019 data (STWSI 2003–2019). Black dots indicate where correlations were not statistically significant.

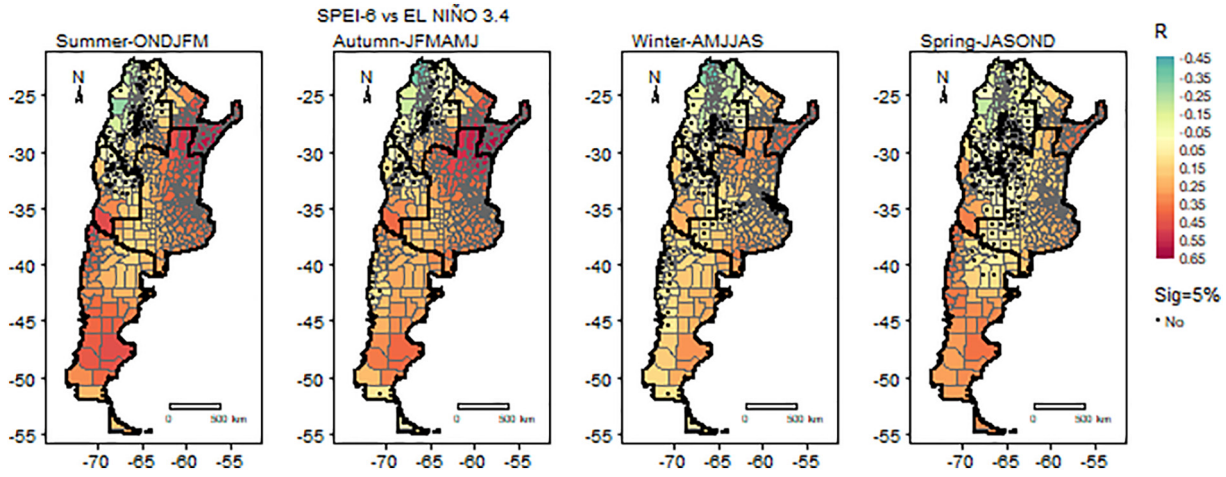

Fig. 5. Spatial pattern of correlations between the seasonal time series SPEI-6 and El Niño 3.4 based on 1982–2019 data.

4. Discussion

4.1. Drought indices and teleconnections

CIs located in the equatorial Pacific Ocean (Tahiti, SOI, El Niño 3.4, and El Niño 4) showed stronger correlations with the DIs in Argentina. Although relatively low r values were found for this type of study, they can be considered acceptable (Lovino et al., 2018; Robledo et al., 2013). These CIs have been found to indicate the triggering of droughts in other parts of the world (Gupta and Jain, 2021; Vicente-Serrano et al., 2017), demonstrating the global importance of their variability in extreme hydrological events. On a larger time scale (12 months), correlations were persistently higher, something that has also been found in other studies (Lovino et al., 2018; Singh and Shukla, 2020). However, it might be possible to find stronger relationships on other time scales, although this was not investigated in the present study. Some DIs (i.e., SSI and SVCI) showed strong correlations with other CIs, which suggests that the explanations for droughts in Argentina are highly complex and cannot be covered by a single climate driver.

Stronger negative correlations between CIs and DIs were found in warm seasons, whereas in cold seasons they were less strong yet positive. These findings coincide with the results in Hurtado and Agosta (2020) and De La Casa and Ovando (2006), in which the climatic drivers were better correlated with the characteristic patterns of the summer than with the winter rainfall regime. Such results, then, suggest that extremely hot and humid summers and extremely dry and cold winters are associated with the variability of these CIs, and may be used for monitoring and forecasting droughts in Argentina, similar to other regions (Dikshit et al., 2021; Seibert et al., 2017).

Spatially, the DIs and CIs showed a stronger correlation in regions with high rainfall regimes and high temperature variability (Pampas and NEA), where the climate classification is semi-arid (temperate climate) according to the Köppen-Geiger climate classification (Kottek et al., 2006). The weakest correlations were found in the arid regions (NEA and north of Cuyo). In the Patagonia region, where the climate is cold, correlations were persistently weaker throughout the year. Similar results have been obtained by Robledo et al. (2013), who found stronger relations between drought conditions and climate drivers in the northeast and central regions of Argentina than in the south. In these regions, CIs might be used in conjunction with other variables (e.g., measurements of streamflow in rivers, water levels in lakes or reservoirs, or snow cover) to better monitor and predict droughts. The reader is referred to Hao et al., 2018 for a review of commonly used predictors for statistical drought prediction.

The spatial patterns of correlations between DIs and CIs indicated that the five administrative regions used were not the most suitable for drought monitoring based on climate drivers (Fig. 5). Therefore, at the national level, we believe that it is necessary to define the climate drivers of droughts in homogeneous drought regions. As an example, Fig. 7 sets out how four regions, based on correlations, can be defined: i) northern Patagonia + eastern Pampas + southern NEA; ii) northern NWA; iii) western Cuyo and Patagonia; and iv) the central part of the country from central NWA to northern Patagonia across eastern Cuyo and western Pampas. The precise definition of homogeneous drought regions is, however, beyond the scope of this work. Specific clustering methodologies, such as principal component analysis and hierarchical and non-hierarchical clustering methods, should be used to establish this regionalisation, ensuring a robust definition of drought regions. These techniques could be applied to identify patterns in the DI and CI series, hence defining regions with similar drought variability and characteristics, as done for example in Espinosa et al. (2019).

Because each DI is associated with a specific part of the water cycle, and it is not common for the entire water cycle also to be under stress at the time due to the drought development process (from meteorological to hydrological) (Huang et al., 2017; Mishra and Singh, 2010), the DIs showed different relationship levels with the CIs. Nevertheless, the STWSI (associated with the total amount of water in the environment, both ground and surface) was notable, showing strong correlations with all CIs. It was also interesting that STWS showed stronger correlations with CIs in the cold than in the hot seasons. This is possibly due to the time lag between hydrological droughts and agricultural and meteorological droughts (Huang et al., 2017; Van Loon, 2015). However, although STWSI primary variables (GRACE data) have been used to successfully detect some significant drought events in Argentina (Chen et al., 2010; Aragón et al., 2011), to claim that the STWSI is the DI that best correlates with the CIs may imply a bias, due to the short time that its data have been available. Thus, a longer time series needs to be used to verify these results.

The STCI, SPEI, and SVHI showed high percentages of departments with significant correlations with CIs (better than the percentage obtained by STWSI, this perhaps due to the length of the time series), indicating that they could be used throughout the country, despite having a lower correlation than the STWSI. These DIs all include temperature in their calculus, which is a very important variable in the relationship between droughts and climate drivers, especially in Argentina (Carcedo and Gambin, 2019). Furthermore, the SPEI showed the strongest correlations with the CIs in the analysis based on soybean-producing departments (Fig. 1c), particularly with El Niño 3.4, and specifically for warm seasons (the growing season for crops such as soybeans). These findings might be of particular interest to drought managers and farmers in Argentina. Further research could define CIs, such as El Niño 3.4, as predictors of agricultural drought in this area.

Table 2
Median correlations between DIs and CIs aggregated for 12 months based on all departments (m = 525) and 1982–2019 (STWSI 2003–2019). Percentage of departments with significant correlation at 5% level ($\rho \leq 0.05$) are showed.

DI		Darwin	Tahiti	Niño3.4	Niño3	Niño4	Niño1 + 2	SOI	PDO	CAR	SWIO	WTIO	SETIO	DMI	TNA	TSA	NAT	SAT	TASI	NAO
SPI-12	*	0.18	−0.33	0.24	0.19	0.23	0.18	−0.27	−0.01	−0.03	0.09	−0.02	0.08	−0.05	−0.13	−0.16	−0.07	−0.09	−0.13	0.11
	**	88.2	85.9	77.0	89.1	74.1	75.6	87.2	55.2	65.9	48.6	65.7	61.3	49.1	75.0	82.5	42.9	49.3	70.1	57.1
SPEI-12	*	0.21	−0.36	0.24	0.21	0.20	0.21	−0.29	0.04	−0.03	0.12	−0.01	0.09	−0.07	−0.15	−0.11	−0.07	−0.05	−0.08	0.10
	**	90.1	86.3	84.0	90.1	79.8	79.6	86.9	64.6	53.3	55.8	57.9	65.9	48.6	77.3	63.0	43.4	31.6	41.9	55.4
SSI-12	*	0.07	−0.06	0.07	0.13	0.04	0.22	−0.08	−0.10	0.32	0.06	0.13	−0.04	0.23	0.15	0.04	0.07	0.00	−0.02	−0.16
	**	40.8	48.8	43.6	74.7	39.4	86.9	49.7	61.5	94.3	50.5	82.5	38.9	89.7	71.2	31.0	57.3	14.9	18.1	83.8
SVCI-12	*	0.02	−0.09	0.11	0.10	0.14	0.04	−0.06	−0.03	0.21	0.02	0.11	0.11	0.01	0.14	−0.01	0.08	−0.01	−0.01	−0.07
	**	51.8	73.7	60.8	60.4	67.2	38.5	68.2	39.4	81.5	41.9	59.0	61.9	44.6	69.5	42.3	53.9	23.8	30.7	54.5
STCI-12	*	0.34	−0.43	0.28	0.29	0.17	0.26	−0.42	0.20	−0.13	0.04	−0.07	0.02	−0.10	−0.28	−0.24	−0.18	−0.13	−0.16	0.27
	**	97.1	98.9	93.9	95.6	89.3	97.3	99.0	85.9	64.8	25.7	50.1	25.9	55.6	94.7	95.6	81.1	78.3	86.3	95.6
SVHI-12	*	0.24	−0.34	0.25	0.25	0.20	0.20	−0.32	0.11	0.03	0.05	0.03	0.09	−0.06	−0.12	−0.17	−0.08	−0.08	−0.10	0.16
	**	91.6	91.0	93.3	93.5	86.5	90.3	92.8	59.8	53.1	41.5	49.5	52.4	47.2	68.4	76.4	55.8	49.0	56.8	75.6
STWSI-12	*	0.40	−0.37	0.38	0.30	0.48	0.25	−0.42	0.54	0.49	0.02	0.40	0.21	0.08	−0.17	0.25	−0.03	0.11	0.16	0.31
	**	86.9	87.6	86.1	78.9	88.6	83.4	92.4	90.9	87.2	14.7	89.0	69.3	60.8	59.4	81.0	21.0	36.0	62.7	85.0
SPDSI-12	*	0.15	−0.30	0.18	0.12	0.16	0.15	−0.27	0.06	0.01	0.06	−0.03	0.08	−0.06	−0.19	−0.10	−0.15	−0.06	−0.08	0.07
	**	73.5	83.8	73.0	71.2	78.5	70.9	81.7	69.1	73.0	37.1	69.0	60.4	47.0	68.2	60.2	62.7	33.3	46.7	45.0

* r.
** Percentage of departments with 5% significance level.
Relevant information is displayed in italics.

Table 3
Median correlations between DIs and CIs aggregated for 12 months based on the departments of Cuyo (m = 44) Patagonia (m = 53), Pampas (m = 233), NEA (m = 76), and NWA (m = 119) and 1982–2019 data (STWSI 2003–2019).

DI	CI	Region				
		Cuyo	Patagonia	Pampas	NEA	NWA
SPI-12	Tahiti SLP	−0.009	−0.319	−0.376	*−0.533*	−0.094
SPEI-12		−0.083	−0.397	−0.375	*−0.505*	−0.010
SSI-12		−0.004	0.067	−0.085	*−0.116*	−0.056
SVCI-12		0.112	−0.075	−0.189	*−0.027*	0.147
STCI-12		−0.433	−0.369	−0.481	*−0.399*	−0.360
SVHI-12		−0.247	−0.350	−0.407	*−0.263*	−0.130
STWSI-12		−0.263	−0.330	−0.545	*−0.346*	−0.076
SPDSI-12		−0.263	−0.330	−0.545	*−0.346*	−0.076
SPI-12	El Niño 3.4	0.045	0.235	0.250	*0.501*	0.049
SPEI-12		0.075	0.250	0.262	*0.478*	−0.021
SSI-12		0.015	0.064	0.092	*0.141*	0.050
SVCI-12		0.032	0.185	0.157	*0.061*	−0.044
STCI-12		0.295	0.204	0.301	*0.330*	0.239
SVHI-12		0.274	0.299	0.273	*0.255*	0.137
STWSI-12		0.087	0.225	0.502	*0.438*	0.228
SPDSI-12		0.087	0.225	0.502	*0.438*	0.228
SPI-12	El Niño 4	−0.106	0.181	0.326	*0.390*	−0.050
SPEI-12		−0.055	0.169	0.303	*0.363*	−0.128
SSI-12		−0.007	0.105	0.059	*0.083*	−0.014
SVCI-12		0.089	0.194	0.172	*0.121*	0.050
STCI-12		0.143	0.134	0.217	*0.251*	0.115
SVHI-12		0.176	0.236	0.230	*0.214*	0.081
STWSI-12		0.148	0.338	0.610	*0.519*	0.246
SPDSI-12		0.148	0.338	0.610	*0.519*	0.246
SPI-12	SOI	−0.092	−0.328	−0.283	*−0.499*	−0.109
SPEI-12		−0.152	−0.387	−0.303	*−0.474*	−0.027
SSI-12		−0.014	0.006	−0.094	*−0.132*	−0.068
SVCI-12		0.069	−0.121	−0.148	*0.032*	0.146
STCI-12		−0.466	−0.358	−0.452	*−0.377*	−0.355
SVHI-12		−0.336	−0.373	−0.362	*−0.221*	−0.153
STWSI-12		−0.275	−0.332	−0.567	*−0.411*	−0.196
SPDSI-12		−0.275	−0.332	−0.567	*−0.411*	−0.196

4.2. Drought indices and soybean yield variability

This study has indicated that the utilisation of a cross-section model resulted in the highest R^2, followed by the time-series model. Such a pattern of results between statistical models is consistent with the results shown in Lobell and Burke (2010). However, statistical models based on a time-series show a better spatial understanding of the relationship between drought and crop yield, which was expected, since having subnational data would a priori provide better approximations (Lobell and Burke, 2010).

The time-series model allowed us to identify areas (or departments) in which soybeans were more sensitive to drought. Soybeans responded better to the SVHI in departments where yields were higher (explaining up to 88.8% of agricultural variability). These areas are located in the north of the Buenos Aires Province (Fig. 8). DIs based on vegetation condition variables (e.g., SVHI) have been associated with crop variability with other crop yields. For instance, in Spain, García-León et al. (2019)

Table 4
Median correlations between DIs and the selected CIs (Tahiti SLP, El Niño 3.4, El Niño 4 and SOI) aggregated for 6 months based on soybean producing departments (m = 193) and 1982–2019 data (STWSI 2003–2019).

DI		Tahiti	El Niño 3.4	El Niño 4	SOI
SPI-6	Summer-ONDJFM	−0.29	0.35	0.38	−0.34
SPEI-6		*−0.29*	*0.37*	*0.38*	*−0.35*
SSI-6		−0.12	0.03	−0.03	−0.15
SPDSI-6		−0.16	0.10	0.13	−0.14
SVCI-6		−0.20	0.22	0.24	−0.23
STCI-6		−0.27	0.29	0.33	−0.35
SVHI-6		−0.26	0.28	0.32	−0.32
STWSI-6		*−0.32*	*0.28*	*0.40*	*−0.41*

Table 5
Determination coefficient results of the a) time-series model (medians), b) panel model, and c) cross-section model between the DIs and soybean yield based on soybean-producing departments (m = 193) and 2004–2019 data.

a)					b)					c)				
R^2 - time-series model	3-Months JFM	3-Months OND	6-Months ONDJFM	12-Months year	R^2 - panel model	3-Months JFM	3-Months OND	6-Months ONDJFM	12-Months year	R^2 - cross-section model	3-Months JFM	3-Months OND	6-Months ONDJFM	12-Months year
SPI	0.188	0.148	*0.298*	0.268	SPI	0.128	0.071	*0.175*	0.154	SPI	0.380	0.196	*0.504*	0.504
SPEI	0.233	0.160	*0.313*	0.253	SPEI	0.160	0.072	*0.174*	0.148	SPEI	0.437	0.220	*0.503*	0.482
SSI	0.195	0.024	*0.142*	0.247	SSI	0.207	0.021	*0.062*	0.157	SSI	0.255	0.003	*0.119*	0.346
SPDSI	0.335	0.016	*0.152*	0.173	SPDSI	0.176	0.000	*0.065*	0.087	SPDSI	0.608	0.007	*0.228*	0.262
SVCI	0.575	0.134	*0.467*	0.333	SVCI	0.268	0.073	*0.234*	0.185	SVCI	0.847	0.470	*0.771*	0.504
STCI	0.556	0.215	*0.452*	0.345	STCI	0.319	0.119	*0.275*	0.262	STCI	0.743	0.475	*0.631*	0.507
SVHI	0.625	0.199	*0.494*	0.416	SVHI	0.324	0.106	*0.276*	0.274	SVHI	0.821	0.511	*0.711*	0.549
STWSI	0.249	0.094	*0.189*	0.204	STWSI	0.195	0.040	*0.143*	0.161	STWSI	0.392	0.139	*0.288*	0.286

found better responses in wheat, barley, oat, rye and maize to the VHI (non-standardised SVHI), and in Argentina, Seiler et al. (2007) explained corn yield variability with the VCI and TCI (non-standardised SVHI SVCI and STCI). The SPEI, on the other hand, accurately explains areas with low yields in the south and north of the soybean belt (up to 71.5% of variability). The SPEI has also been widely associated with the response of crop yields to droughts (Chen et al., 2016; Peña-Gallardo et al., 2019a). Interestingly, the STWSI, which has a strong relationship with the CIs, performed poorly in explaining soybean responses to droughts, which can be explained by the fact that this index is associated with longer drought timescales, more representative of hydrological droughts (reservoirs, aquifers, etc.) than meteorological or agricultural droughts (Zhou et al., 2020).

The findings also indicate that CIs explain variability in soybean yield very poorly. This does not necessarily mean that climate drivers and crop (soybean) production are not associated. Relations between ENSO and crop yields have been established by Anderson et al. (2018) and Podestá et al. (1999). Furthermore, in this study, we analysed three timescales (3, 6, and 12 months) for specific months (December, March, and June); therefore, an extension of this study using a variety of different time scales may be necessary to verify the results. However, for the purposes of annual/seasonal monitoring of soybean production in Argentina, based on our results, we recommend using a DI rather than a CI.

One of the limitations of this study was the lack of data associated with irrigation. In areas with purely rainfed crops, meteorological variables are more important for crop development (Kuwayama et al., 2018). Therefore, the disparity in the results using the SPEI and SVHI could be attributed to the fact that in areas with higher yields, there might have been some type of additional irrigation. According to (FAO et al., 2015), there are some small-scale irrigated areas irrigated fields in the northern Buenos Aires Province. This should be studied in detail in each departmental unit. In other locations, crops (including soybeans) usually have short time dependencies (1–4 months) (Peña-Gallardo et al., 2018). In future studies, it will be necessary to refine the analysis of the link between soybean yields and droughts using various other time scales, for instance, following the methodology used by Peña-Gallardo et al. (2019b) in the United States. However, at the national level, but with a focus on specific regions, the use of SPEI and SVHI aggregated for 3 and 6 months during phenological growth to monitor the state of soybean production is recommended. This information might prove useful for local farmers.

5. Conclusions

In this study, 8 DIs, and 19 CIs were benchmarked for agricultural drought monitoring in Argentina. First, the relationship between DIs and CIs was explored. Then, DIs were evaluated based on their capacity to explain the impacts of agricultural drought (annual soybean yield variability). Finally, the best response of crop production to DIs, rather than to CIs, was presented.

DIs were particularly related to the CIs located in the Pacific Ocean, including El Niño 3.4 and El Niño 4. DIs that include temperature in their computation (STCI, SPEI, and SVHI) correlated best with CIs across the country. For soybean production areas, SPEI was the DI that best responded to variations in CIs. Correlations were positive and strong in the warm and wet season (summer), while in the cold and dry season (winter), they were negative and less strong. Droughts were strongly linked to the CIs defined in some Argentinian regions.

The time series model showed a sound spatial characterization of the relationship between drought and crop yield. Soybean yield variability (impacts associated with agricultural droughts) responded better to DIs than to CIs. The SVHI and SPEI aggregated for 6 months and corresponding to the month of March (soybean growth season) were found to best explain the state of soybean production in certain regions.

The results provide useful drought insight tools in various parts of the water cycle and their association with variability in soybean

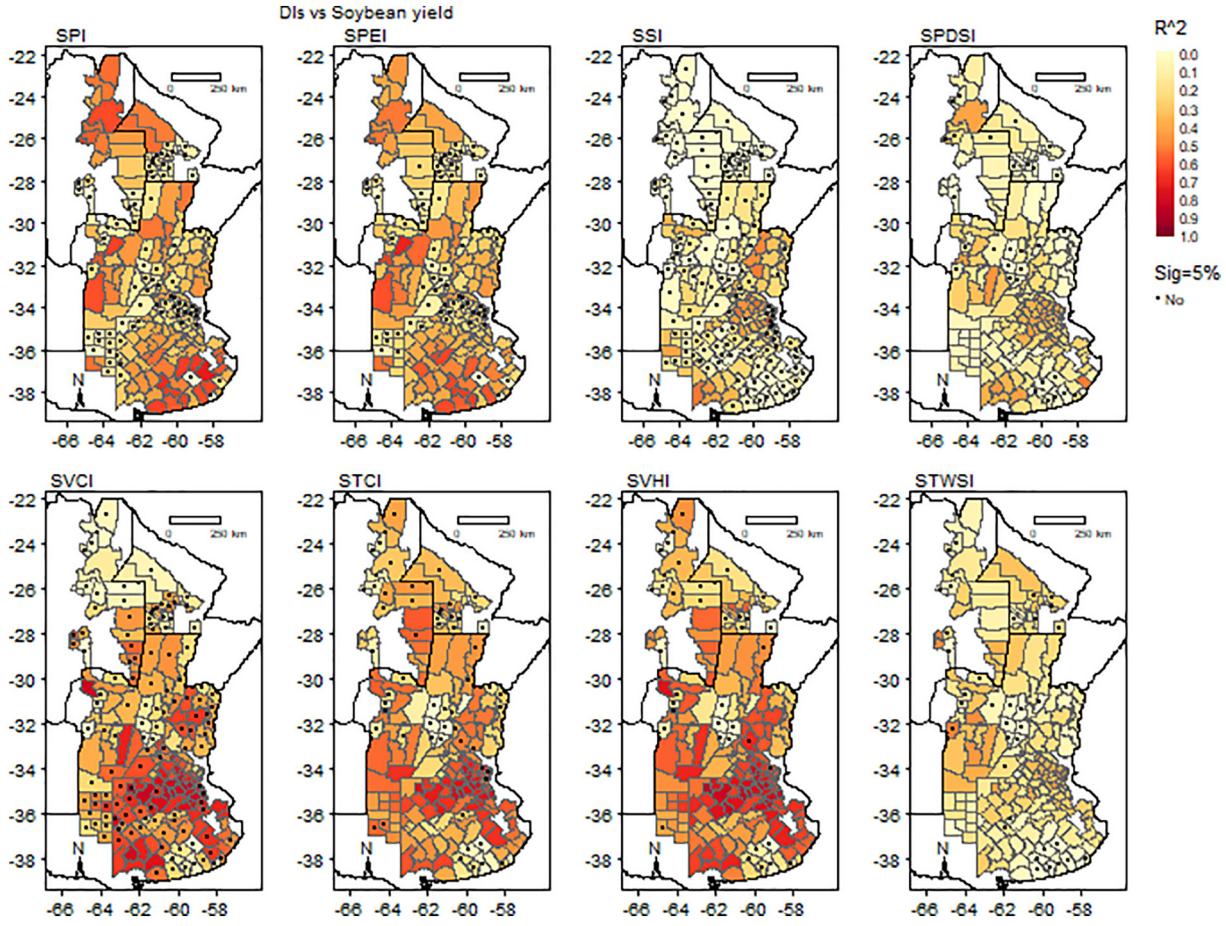

Fig. 6. Spatial patterns of the determination coefficient results of the time-series models between DIs aggregated 6 months (ONDJFM) and soybean yield based on soybean-producing departments (m = 193) and 2004–2019 data.

Table 6
Median correlations between the selected CIs (Tahiti SLP, El Niño 3.4, El Niño 4 and SOI) aggregated for 3,6, and 12 months and the soybean yield based on soybean-producing departments (m = 193) and 2004–2019 data.

R^2 - Time-series model	3-Months JFM	3-Months OND	6-Months ONDJFM	12-Months year
El Niño 3.4	*0.087*	0.074	0.073	0.004
SOI	0.129	0.025	*0.044*	0.000
TAHITI	0.110	0.110	*0.027*	0.015
El Niño 4	0.119	0.082	*0.063*	0.002

production in Argentina Therefore, this research might be of interest to water managers and especially soybean producers, at national and regional level in Argentina. It may also serve as a foundation for future studies on drought in Argentina. It would be particularly interesting to explore the predictive rather than the explanatory capacity of the selected DIs and CIs for forecasting droughts in the country. The methodology is also of general applicability and relies on freely global-scale datasets, so it could be replicated in other regions of the world.

Supplementary data to this article can be found online at https://doi.org/10.1016/j.scitotenv.2021.148090.

CRediT authorship contribution statement

Ronnie J. Araneda-Cabrera: Conceptualization, Methodology, Software, Formal analysis, Investigation, Data curation, Writing – original draft, Visualization. **María Bermudez:** Conceptualization, Validation, Formal analysis, Writing – review & editing, Supervision. **Jerónimo Puertas:** Conceptualization, Resources, Writing – review & editing, Supervision.

Declaration of competing interest

The authors declare that they have no known competing financial interests or personal relationships that could have appeared to influence the work reported in this paper.

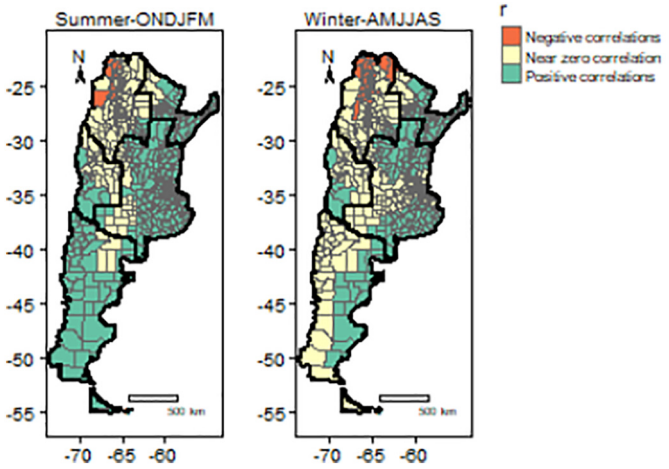

Fig. 7. Spatial distribution of positive (r > 0.2), negative (r < −0.2), and near zero (−0.2 ≤ r ≤ 0.2) correlations between SPEI-6 and the El Niño 3.4. The black lines show the regional divisions.

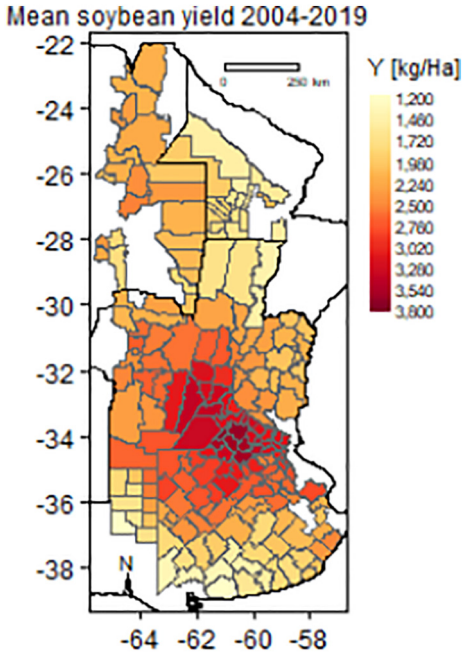

Fig. 8. Spatial distribution of average annual soybean yield (period 2004–2019).

Acknowledgements

Ronnie Araneda gratefully acknowledges financial support from the Spanish Regional Government of Galicia (Xunta de Galicia) and the European Union through the predoctoral grant reference ED481A-2018/162. María Bermúdez was supported by the European Union H2020 Research and Innovation Program under the Marie Skłodowska-Curie Grant Agreement No. 754446 and the Research and Transfer Fund of the University of Granada - Athenea3i.

References

Abatzoglou, J.T., Dobrowski, S.Z., Parks, S.A., Hegewisch, K.C., 2018. TerraClimate, a high-resolution global dataset of monthly climate and climatic water balance from 1958-2015. Sci. Data 5, 1–12. https://doi.org/10.1038/sdata.2017.191.

Agutu, N.O., Awange, J.L., Zerihun, A., Ndehedehe, C.E., Kuhn, M., Fukuda, Y., 2017. Assessing multi-satellite remote sensing, reanalysis, and land surface models' products in characterizing agricultural drought in East Africa. Remote Sens. Environ. 194, 287–302. https://doi.org/10.1016/j.rse.2017.03.041.

Anderson, W., Seager, R., Baethgen, W., Cane, M., 2017. Life cycles of agriculturally relevant ENSO teleconnections in North and South America. Int. J. Climatol. 37, 3297–3318. https://doi.org/10.1002/joc.4916.

Anderson, W., Seager, R., Baethgen, W., Cane, M., 2018. Trans-Pacific ENSO teleconnections pose a correlated risk to agriculture. Agric. For. Meteorol. 262, 298–309. https://doi.org/10.1016/j.agrformet.2018.07.023.

Aragón, R., Jobbágy, E.G., Viglizzo, E.F., 2011. Surface and groundwater dynamics in the sedimentary plains of the Western Pampas (Argentina). Ecohydrology 4, 433–447. https://doi.org/10.1002/eco.149.

Araneda-Cabrera, R.J., Bermúdez, M., Puertas, J., 2020. Unified framework for drought monitoring and assessment in a transboundary river basin. In: Uijttewaal, W., Franca, M., Valero, D., Chavarrias, V., Arbós, C., Schielen, R., Crosato, A. (Eds.), River Flow 2020. Taylor & Francis Group, London, pp. 1081–1086 https://doi.org/10.1201/b22619.

Araneda-Cabrera, R.J., Bermúdez, M., Puertas, J., 2021. Assessment of the performance of drought indices for explaining crop yield variability at the national scale: methodological framework and application to Mozambique. Agric. Water Manag. 246. https://doi.org/10.1016/j.agwat.2020.106692.

Barros, V.R., Silvestri, G.E., 2002. The relation between sea surface temperature at the subtropical South-Central Pacific and precipitation in Southeastern South America. J. Clim. 15, 251–267. https://doi.org/10.1175/1520-0442(2002)015<0251:trbsst>2.0.co;2.

Beck, H.E., Zimmermann, N.E., McVicar, T.R., Vergopolan, N., Berg, A., Wood, E.F., 2018. Present and future köppen-geiger climate classification maps at 1-km resolution. Sci. Data 5, 1–12. https://doi.org/10.1038/sdata.2018.214.

Carcedo, A.J.P., Gambin, B.L., 2019. Sorghum drought and heat stress patterns across the Argentinean temperate central region. Field Crops Res. 241, 107552. https://doi.org/10.1016/j.fcr.2019.06.009.

Chen, J.L., Wilson, C.R., Tapley, B.D., Longuevergne, L., Yang, Z.L., Scanlon, B.R., 2010. Recent la Plata basin drought conditions observed by satellite gravimetry. J. Geophys. Res. Atmos. 115, 1–12. https://doi.org/10.1029/2010JD014689.

Chen, T., Xia, G., Liu, T., Chen, W., Chi, D., 2016. Assessment of drought impact on main cereal crops using a standardized precipitation evapotranspiration index in Liaoning Province, China. Sustain. 8, 1–16. https://doi.org/10.3390/su8101069.

Cherlet, M., Hutchinson, Charles, Reynolds, J., Hill, J., Sommer, S., Von Maltitz, G., 2018. World Atlas of Desertification. Rethinking Land Degradation and Sustainable Land Management. Third Edit. Publications Office of the European Union https://doi.org/10.2760/06292.

D'Ambrosio, G.T., Bohn, V.Y., Piccolo, M.C., 2013. Evaluation of the 2008-2009 drought in the west of the Pampean region (Argentina). Cuad. Geogr. 52, 29–45.

De La Casa, A.C., Ovando, G.G., 2006. The influence of El Niño Southern Oscillation (ENSO) episodes on rainfall and corn yields in Córdoba Province, Argentina. Agric. Técnica 66, 80–89. https://doi.org/10.4067/S0365-28072006000100009.

Díaz, E., García, M., Rodríguez, A., Dölling, O., Ochoa, S., Bertoni, J., 2018. Temporal evolution of hydrological drought in Argentina and its relationship with macroclimatic indicators. Tecnol. Cienc. Agua 9, 1–32. https://doi.org/10.24850/j-tyca-2018-05-01.

Dikshit, A., Pradhan, B., Alamri, A.M., 2021. Long lead time drought forecasting using lagged climate variables and a stacked long short-term memory model. Sci. Total Environ. 755, 142638. https://doi.org/10.1016/j.scitotenv.2020.142638.

Dorigo, W., Wagner, W., Albergel, C., Albrecht, F., Balsamo, G., Brocca, L., Chung, D., Ertl, M., Forkel, M., Gruber, A., Haas, E., Hamer, P.D., Hirschi, M., Ikonen, J., de Jeu, R., Kidd, R., Lahoz, W., Liu, Y.Y., Miralles, D., Mistelbauer, T., Nicolai-Shaw, N., Parinussa, R., Pratola, C., Reimer, C., van der Schalie, R., Seneviratne, S.I., Smolander, T., Lecomte, P., 2017. ESA CCI soil moisture for improved Earth system understanding: state-of-the art and future directions. Remote Sens. Environ. 203, 185–215. https://doi.org/10.1016/j.rse.2017.07.001.

Dutra, E., Di Giuseppe, F., Wetterhall, F., Pappenberger, F., 2013. Seasonal forecasts of droughts in African basins using the Standardized Precipitation Index. Hydrol. Earth Syst. Sci. 17, 2359–2373. https://doi.org/10.5194/hess-17-2359-2013.

EM-DAT, 2019. The Emergency Events Database. Universite catholique de Louvain, Brussels, Belgium Available at. http://www.emdat.be/. (Accessed November 2019).

Espinosa, L.A., Portela, M.M., Rodrigues, R., 2019. Spatio-temporal variability of droughts over past 80 years in Madeira Island. J. Hydrol. Reg. Stud. 25, 100623. https://doi.org/10.1016/j.ejrh.2019.100623.

FAO, 2016. Regional roundtable on the World Programme for the Census of Agriculture 2020 (WCA 2020). 12-16 December 2016, Montevideo, Uruguay. World Programme for the Census of Agriculture [online]. Rome, Italy. http://www.fao.org/world-census-agriculture/events/wca2020montevideo/en/.

FAO, 2017. Country fact sheet on food and agriculture policy trends. Argentina, Food and Agriculture Organization of the United Nations. I7752EN/1/08.17.

FAO, PROSAP, Ministerio de Agricultura Ganadería y Pesca de Argentina, 2015. Estudio del potencial de ampliación del riego en Argentina. Buenos Aires. http://www.fao.org/3/a-i5183s.pdf.

FAO, 2019. World Food and Agriculture – Statistical pocketbook 2019 Rome.

García-León, D., Contreras, S., Hunink, J., 2019. Comparison of meteorological and satellite-based drought indices as yield predictors of Spanish cereals. Agric. Water Manag. 213, 388–396. https://doi.org/10.1016/j.agwat.2018.10.030.

Golnaraghi, M., Etienne, C., Sapir, D.G., Below, R., 2014. Atlas of mortality and economic losses from weather. Climate and Water Extremes (1970–2012), WMO-No. 1123. World Meteorological Organization, Geneva, Switzerland https://www.preventionweb.net/files/38413_wmo1123atlas120614.pdf.

Gupta, V., Jain, M.K., 2021. Unravelling the teleconnections between ENSO and dry/wet conditions over India using nonlinear Granger causality. Atmos. Res. 247, 105168. https://doi.org/10.1016/j.atmosres.2020.105168.

Guttman, N.B., 1998. Comparing the palmer drought index and the standardized precipitation index. J. Am. Water Resour. Assoc. 34, 113–121. https://doi.org/10.1111/j.1752-1688.1998.tb05964.x.

Hao, Z., AghaKouchak, A., 2013. Multivariate Standardized Drought Index: a parametric multi-index model. Adv. Water Resour. 57, 12–18. https://doi.org/10.1016/j.advwatres.2013.03.009.

Hao, Z., AghaKouchak, A., 2014. A nonparametric multivariate multi-index drought monitoring framework. J. Hydrometeorol. 15, 89–101. https://doi.org/10.1175/JHM-D-12-0160.1.

Hao, Z., Singh, V.P., Xia, Y., 2018. Seasonal drought prediction: advances, challenges, and future prospects. Rev. Geophys. 56, 108–141. https://doi.org/10.1002/2016RG000549.

Hassan, W.U., Nayak, M.A., 2020. Global teleconnections in droughts caused by oceanic and atmospheric circulation patterns. Environ. Res. Lett. 16. https://doi.org/10.1088/1748-9326/abc9e2.

Huang, S., Huang, Q., Leng, G., Liu, S., 2016. A nonparametric multivariate standardized drought index for characterizing socioeconomic drought: a case study in the Heihe River Basin. J. Hydrol. 542, 875–883. https://doi.org/10.1016/j.jhydrol.2016.09.059.

Huang, S., Li, P., Huang, Q., Leng, G., Hou, B., Ma, L., 2017. The propagation from meteorological to hydrological drought and its potential influence factors. J. Hydrol. 547, 184–195. https://doi.org/10.1016/j.jhydrol.2017.01.041.

Hurtado, S.I., Agosta, E.A., 2020. El Niño Southern Oscillation-related precipitation anomaly variability over eastern subtropical South America: atypical precipitation seasons. Int. J. Climatol. 1–20. https://doi.org/10.1002/joc.6559.

Iizumi, T., Luo, J.J., Challinor, A.J., Sakurai, G., Yokozawa, M., Sakuma, H., Brown, M.E., Yamagata, T., 2014. Impacts of El Niño Southern Oscillation on the global yields of major crops. Nat. Commun. 5, 1–7. https://doi.org/10.1038/ncomms4712.

Keyantash, J., Dracup, J.A., 2002. Quantification of drought an evaluation of drought indices. Am. Meteorol. Soc., 1167–1180 https://doi.org/10.1175/1520-0477-83.8.1167.

Kogan, F.N., 1995. Application of vegetation index and brightness temperature for drought detection. Adv. Space Res. 15, 91–100. https://doi.org/10.1016/0273-1177(95)00079-T.

Kottek, M., Grieser, J., Beck, C., Rudolf, B., Rubel, F., 2006. World map of the Köppen-Geiger climate classification updated. Meteorol. Z. 15, 259–263. https://doi.org/10.1127/0941-2948/2006/0130.

Kumar, N.M., Murthy, C.S., Sesha Sai, M.V.R., Roy, P.S., 2009. On the use of Standardized Precipitation Index (SPI) for drought intensity assessment. Meteorol. Appl. 16, 381–389. https://doi.org/10.1002/met.136.

Kuwayama, Y., Thompson, A., Bernknopf, R., Zaitchik, B., Vail, P., 2018. Estimating the impact of drought on agriculture using the U.S. drought monitor. Am. J. Agric. Econ. 101, 193–210. https://doi.org/10.1093/ajae/aay037.

Landerer, F.W., Swenson, S.C., 2012. Accuracy of scaled GRACE terrestrial water storage estimates. Water Resour. Res. 48, 1–11. https://doi.org/10.1029/2011WR011453.

Landerer, F.W., Flechtner, F.M., Save, H., Webb, F.H., Bandikova, T., Bertiger, W.I., Bettadpur, S.V., Byun, S.H., Dahle, C., Dobslaw, H., Fahnestock, E., Harvey, N., Kang, Z., Kruizinga, G.L.H., Loomis, B.D., McCullough, C., Murböck, M., Nagel, P., Paik, M., Pie, N., Poole, S., Strekalov, D., Tamisiea, M.E., Wang, F., Watkins, M.M., Wen, H.Y., Wiese, D.N., Yuan, D.N., 2020. Extending the global mass change data record: GRACE follow-on instrument and science data performance. Geophys. Res. Lett. 47, 1–10. https://doi.org/10.1029/2020GL088306.

Leng, G., Hall, J., 2019. Crop yield sensitivity of global major agricultural countries to droughts and the projected changes in the future. Sci. Total Environ. 654, 811–821. https://doi.org/10.1016/j.scitotenv.2018.10.434.

Lobell, D.B., Burke, M.B., 2010. On the use of statistical models to predict crop yield responses to climate change. Agric. For. Meteorol. 150, 1443–1452. https://doi.org/10.1016/j.agrformet.2010.07.008.

Lobell, D.B., Bänziger, M., Magorokosho, C., Vivek, B., 2011a. Nonlinear heat effects on African maize as evidenced by historical yield trials. Nat. Clim. Chang. 1, 42–45. https://doi.org/10.1038/nclimate1043.

Lobell, D.B., Schlenker, W., Costa-Roberts, J., 2011b. Climate trends and global crop production since 1980. Science (80-.) 333, 616–621. https://doi.org/10.7551/mitpress/8876.003.0036.

Lovino, M.A., Müller, O.V., Müller, G.V., Sgroi, L.C., Baethgen, W.E., 2018. Interannual-to-multidecadal hydroclimate variability and its sectoral impacts in northeastern Argentina. Hydrol. Earth Syst. Sci. 22, 3155–3174. https://doi.org/10.5194/hess-22-3155-2018.

Ma, M., Ren, L., Yuan, F., Jiang, S., Liu, Y., Kong, H., Gong, L., 2014. A new standardized Palmer drought index for hydro-meteorological use. Hydrol. Process. 28, 5645–5661. https://doi.org/10.1002/hyp.10063.

Magrin, G.O., Travasso, M.I., Rodríguez, G.R., 2005. Changes in climate and crop production during the 20th century in Argentina. Clim. Chang. 72, 229–249. https://doi.org/10.1007/s10584-005-5374-9.

Manatsa, D., Chingombe, W., Matsikwa, H., Matarira, C.H., 2008. The superior influence of Darwin Sea level pressure anomalies over ENSO as a simple drought predictor for Southern Africa. Theor. Appl. Climatol. 92, 1–14. https://doi.org/10.1007/s00704-007-0315-3.

McKee, T.B., Doesken, N.J., Kleist, J., 1993. The Relationship of Drought Frequency and Duration to Time Scales, Paper Presented at 8th Conference on Applied Climatology. American Meteorological Society, Anaheim, CA https://doi.org/10.1088/1755-1315/5.

Mishra, A.K., Singh, V.P., 2010. A review of drought concepts. J. Hydrol. 391, 202–216. https://doi.org/10.1016/j.jhydrol.2010.07.012.

Noor, N.M., Al Bakri Abdullah, M.M., Yahaya, A.S., Ramli, N.A., 2015. Comparison of linear interpolation method and mean method to replace the missing values in environmental data set. Materials Science Forum. Trans Tech Publications Ltd., pp. 278–281 https://doi.org/10.4028/www.scientific.net/MSF.803.278.

Oñate-Valdivieso, F., Uchuari, V., Oñate-Paladines, A., 2020. Large-scale climate variability patterns and drought: a case of study in south – America. Water Resour. Manag. 34, 2061–2079. https://doi.org/10.1007/s11269-020-02549-w.

Palmer, W.C., 1965. Meteorological Drought, Research Paper No. 45. US Weather Bur, Washington, DC, p. 58 p-and-precip/drought/docs/palmer.pdf.

Peña-Gallardo, M., Vicente-Serrano, S.M., Quiring, S., Svodova, M., Hannaford, J., 2018. Effectiveness of drought indices in identifying impacts on major crops across the USA. Clim. Res. 75, 221–240. https://doi.org/10.3354/cr01519.

Peña-Gallardo, M., Martín Vicente-Serrano, S., Domínguez-Castro, F., Beguería, S., 2019a. The impact of drought on the productivity of two rainfed crops in Spain. Nat. Hazards Earth Syst. Sci. 19, 1215–1234. https://doi.org/10.5194/nhess-19-1215-2019.

Peña-Gallardo, M., Vicente-Serrano, S.M., Quiring, S., Svoboda, M., Hannaford, J., Tomas-Burguera, M., Martín-Hernández, N., Domínguez-Castro, F., El Kenawy, A., 2019b. Response of crop yield to different time-scales of drought in the United States: spatio-temporal patterns and climatic and environmental drivers. Agric. For. Meteorol. 264, 40–55. https://doi.org/10.1016/j.agrformet.2018.09.019.

Podestá, G.P., Messina, C.D., Grondona, M.O., Magrin, G.O., 1999. Associations between grain crop yields in Central-Eastern Argentina and El Niño-Southern oscillation. J. Appl. Meteorol. 38, 1488–1498. https://doi.org/10.1175/1520-0450(1999)038<1488:ABGCYI>2.0.CO;2.

Quiring, S.M., Papakryiakou, T.N., 2003. An evaluation of agricultural drought indices for the Canadian prairies. Agric. For. Meteorol. 118, 49–62. https://doi.org/10.1016/S0168-1923(03)00072-8.

Rivera, J.A., Araneo, D.C., Penalba, O.C., Villalba, R., 2018. Regional aspects of streamflow droughts in the Andean rivers of Patagonia, Argentina. Links with large-scale climatic oscillations. Hydrol. Res. 49, 134–149. https://doi.org/10.2166/nh.2017.207.

Robledo, F.A., Penalba, O.C., Bettolli, M.L., 2013. Teleconnections between tropical-extratropical oceans and the daily intensity of extreme rainfall over Argentina. Int. J. Climatol. 33, 735–745. https://doi.org/10.1002/joc.3467.

Rojas, O., Vrieling, A., Rembold, F., 2011. Assessing drought probability for agricultural areas in Africa with coarse resolution remote sensing imagery. Remote Sens. Environ. 115, 343–352. https://doi.org/10.1016/j.rse.2010.09.006.

Santos, M.S., Costa, V.A.F., Fernandes, W.D.S., de Paes, R.P., 2019. Time-space characterization of droughts in the São Francisco river catchment using the Standard Precipitation Index and continuous wavelet transform. Rev. Bras. Recur. Hidr. 24, 1–12. https://doi.org/10.1590/2318-0331.241920180092.

Seibert, M., Merz, B., Apel, H., 2017. Seasonal forecasting of hydrological drought in the Limpopo Basin: a comparison of statistical methods. Hydrol. Earth Syst. Sci. 21, 1611–1629. https://doi.org/10.5194/hess-21-1611-2017.

Seiler, R.A., Kogan, F., Wei, G., Vinocur, M., 2007. Seasonal and interannual responses of the vegetation and production of crops in Cordoba - Argentina assessed by AVHRR derived vegetation indices. Adv. Space Res. 39, 88–94. https://doi.org/10.1016/j.asr.2006.05.024.

Shi, W., Tao, F., Zhang, Z., 2013. A review on statistical models for identifying climate contributions to crop yields. J. Geogr. Sci. 23, 567–576. https://doi.org/10.1007/s11442-013-1029-3.

Singh, R.M., Shukla, P., 2020. Drought characterization using drought indices and El Niño effects. Natl. Acad. Sci. Lett. 43, 339–342. https://doi.org/10.1007/s40009-019-00870-6.

Singh, V.P.E., 2012. Hydrology of Disasters. Springer Science & Business Media https://doi.org/10.1007/978-94-015-8680-1.

Stenseth, N.C., Ottersen, G., Hurrell, J.W., Mysterud, A., Lima, M., Chan, K.S., Yoccoz, N.G., Ådlandsvik, B., 2003. Studying climate effects on ecology through the use of climate indices: the North Atlantic Oscillation, El Niño Southern Oscillation and beyond. Proc. R. Soc. B Biol. Sci. 270, 2087–2096. https://doi.org/10.1098/rspb.2003.2415.

Tan, R., Perkowski, M., 2015. Wavelet-coupled machine learning methods for drought forecast utilizing hybrid meteorological and remotely-sensed data. Proceedings Conference on Data Mining, DMIN15 Http://Archives.Pdx.Edu/Ds/Psu/19370.

Tester, Mark, Langridge, P., 2010. Breeding technologies to increase. Science (80-.) 818, 818–822. https://doi.org/10.1126/science.1183700.

Thomas, A.C., Reager, J.T., Famiglietti, J.S., Rodell, M., 2014. A GRACE-based water storage deficit approach for hydrological drought characterization. Geophys. Res. Lett. Res. 41, 3307–3314. https://doi.org/10.1002/2014GL061184.Received.

Tian, L., Yuan, S., Quiring, S.M., 2018. Evaluation of six indices for monitoring agricultural drought in the south-central United States. Agric. For. Meteorol. 249, 107–119. https://doi.org/10.1016/j.agrformet.2017.11.024.

Van Loon, A.F., 2015. Hydrological drought explained. Wiley Interdiscip. Rev. Water 2, 359–392. https://doi.org/10.1002/wat2.1085.

Vicario, L., García, C.M., Teich, I., Bertoni, J.C., Ravelo, A., Rodríguez, A., 2015. Characterization of meteorological droughts in the central Argentina. Tecnol. Cienc. Agua 6, 153–165.

Vicente-Serrano, S.M., Beguería, S., López-Moreno, J.I., 2010. A multiscalar drought index sensitive to global warming: the standardized precipitation evapotranspiration index. J. Clim. 23, 1696–1718. https://doi.org/10.1175/2009JCLI2909.1.

Vicente-serrano, S.M., Begueri, S., Camarero, J., Lorenzo-lacruz, J., Azorin-molina, C., Lo, J.I., 2012. Performance of drought indices for ecological, agricultural, and hydrological applications. Earth Interact. 16. https://doi.org/10.1175/2012EI000434.1.

Vicente-Serrano, S.M., Martínez, E.A.R., Aguilar, E., Martínez, R., Martín-Hernández, N., Azorin-Molina, C., Sanchez-Lorenzo, A., Kenawy, A. El, Tomás-Burguera, M., Moran-Tejeda, E., López-Moreno, J.I., Revuelto, J., Beguería, S., Nieto, J.J., Drumond, A., Gimeno, L., Nieto, R., 2017. The complex influence of ENSO on droughts in Ecuador. Clim. Dyn. 48, 405–427. https://doi.org/10.1007/s00382-016-3082-y.

Wang, B., Feng, P., Waters, C., Cleverly, J., Liu, D.L., Yu, Q., 2020. Quantifying the impacts of pre-occurred ENSO signals on wheat yield variation using machine learning in Australia. Agric. For. Meteorol. 291, 108043. https://doi.org/10.1016/j.agrformet.2020.108043.

Wang, Y., Liu, G., Guo, E., 2019. Spatial distribution and temporal variation of drought in Inner Mongolia during 1901–2014 using Standardized Precipitation Evapotranspiration Index. Sci. Total Environ. 654, 850–862. https://doi.org/10.1016/j.scitotenv.2018.10.425.

World Meteorological Organization and Global Water Partnership, 2016. In: Svoboda, M., Fuchs, B.A. (Eds.), Handbook of Drought Indicators and Indices. Integrated Drought Management Programme (IDMP), Integrated Drought Management Tools and Guidelines Series 2, Geneva https://doi.org/10.1201/9781315265551-12.

Zampieri, M., Ceglar, A., Dentener, F., Toreti, A., 2017. Wheat yield loss attributable to heat waves, drought and water excess at the global, national and subnational scales. Environ. Res. Lett. 12, 1293. https://doi.org/10.1088/1748-9326/aa723b.

Zargar, A., Sadiq, R., Naser, B., Khan, F.I., 2011. A review of drought indices. Environ. Rev. 19, 333–349. https://doi.org/10.1139/a11-013.

Zhou, W., Guan, K., Peng, B., Shi, J., Jiang, C., Wardlow, B., Pan, M., Kimball, J.S., Franz, T.E., Gentine, P., He, M., Zhang, J., 2020. Connections between the hydrological cycle and crop yield in the rainfed U.S. Corn Belt. J. Hydrol. 590, 125398. https://doi.org/10.1016/j.jhydrol.2020.125398.